Macromolecules

pubs.acs.org/Macromolecules Article

High-Efficient Access to Inverse Morphologies via Living Anionic Polymerization-Mediated Polymerization-Induced Cooperative Assembly

Jingwei Zhang, Peng Zhou, Boyang Shi, Penghan Li, and Guowei Wang*

Cite This: *Macromolecules* 2023, 56, 5743−5753 Read Online

ACCESS | Metrics & More | Article Recommendations | Supporting Information

ABSTRACT: Polymerization-induced cooperative assembly (PICA), originating from polymerization-induced self-assembly, is believed to be a high-efficient method to access higher-order morphologies. Living anionic polymerization (LAP) possesses numerous advantages, such as high monomer conversion, rapid polymerization rate, and excellent controllability. We herein reported a facile strategy to prepare higher-order morphologies using a living anionic polymerization-mediated polymerization-induced cooperative assembly (LAP PICA) process based on polyisoprene-*b*-polystyrene/polystyrene (PS) blends. The morphological transition ranging from spherical micelles to worms, jellyfish, vesicles, sponges, and ordered mesophases of *Im*3*m* cubosomes and *p*6*mm* hexosomes was observed and demonstrated by transmission electron microscopy, field-emission scanning electron microscopy, and small-angle X-ray scattering. Moreover, morphological distribution diagrams including factors, such as the degree of polymerization and content of the PS homopolymer, and solid contents were depicted to unveil the effect of LAP PICA on morphologies and provide guiding principles for preparing a variety of morphologies. Furthermore, a relevant morphological transition mechanism via LAP PICA was put forward.

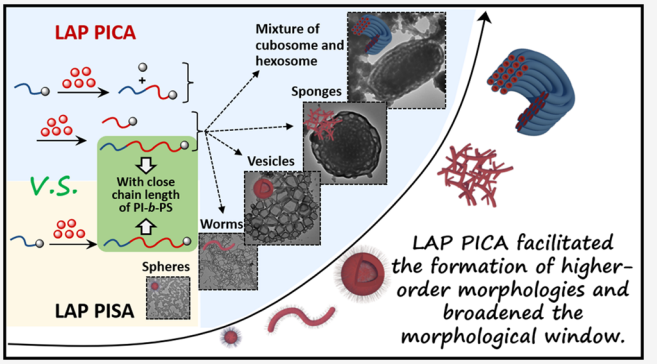

INTRODUCTION

Nano-objects of amphiphilic block copolymers have received undiminished attention for several decades due to their versatile morphologies and promising application in many fields.[1−4] Typically, these nano-objects are prepared by self-assembly of amphiphilic block copolymers in a selective solvent, which has acknowledged limitations of multistep processing and low concentration (<1.0% w/w).[5−7] In contrast, polymerization-induced self-assembly (PISA), integrating a polymerization and in situ self-assembly process, has enabled efficient and reliable access to various morphologies at high concentrations (solid content up to 50% w/w) in recent years.[8−13]

It is generally deemed that the morphology of nano-objects formed under thermodynamical equilibrium is primarily determined by the inherent molecular curvature and packing of copolymer chains as defined by the packing parameter $P = v/a_0 l_c$ (v, a_0, and l_c represent the volume of the core-forming block, the interfacial area, and the length of the core-forming block, respectively).[14] Hence, various morphologies such as spherical, wormlike, laminar, and vesicular micelles ($P \leq 1$) can be captured by adjusting these three parameters to regulate the P value.[13,15−22] However, despite burgeoning development in the PISA process, large compound vesicles, sponges, and inverse bicontinuous mesophases such as cubosomes and hexosomes ($P > 1$) have been rarely reported,[23−30] presumably owing to their intricate formation mechanism and elusive assembly conditions. So far, only three pieces of literature have reported hexosome phases captured in the PISA system.[23,25,29] Nevertheless, nano-objects with high porosity, large specific surface area, and well-ordered network at the nanoscale that endow the materials with high energy dissipation and high ductility have shown great promise in mechanical metamaterials,[31,32] nanonetwork thermosets,[33] biomaterials, nanotemplating,[34,35] and so forth. As a consequence, it is greatly desirable to make full use of the advantages of the self-assembly process to prepare inverse bicontinuous mesophases, which will lay a solid foundation for their further development toward diversification and practicability.

Encouragingly, based on the PISA strategy, a fresh system termed polymerization-induced cooperative assembly (PICA) has been proposed by An and co-workers,[36] in which excellent modulation on nano-object morphologies was achieved

Received: April 20, 2023
Revised: June 29, 2023
Published: July 14, 2023

https://doi.org/10.1021/acs.macromol.3c00759
Macromolecules 2023, 56, 5743−5753

Scheme 1. (a) LAP PICA of St Mediated by PI-*b*-PS$^-$Li$^+$ and *n*-Bu$^-$Li$^+$ in *n*-Heptane; (b) Illustration of Morphologies Prepared via LAP PICA

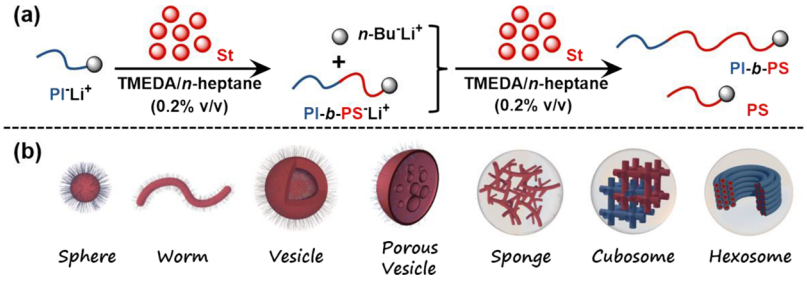

through combining a small molecular reversible addition-fragmentation chain transfer (RAFT) agent and a macro-RAFT agent to simultaneously form a solvophobic homopolymer and an amphiphilic diblock copolymer in the polymerization process. More recently, it has been strongly proven that the PICA process can reliably and effectively accelerate morphological transitions toward higher-order morphologies.[27,36−40] For instance, Zhang and co-workers reported that the compartmentalized vesicles and porous nanospheres can be obtained from self-assembled blends of AB/B or AB/BAB block copolymers.[37,38] A similar method was adopted by Tan et al. to acquire porous spheres[39] and large complex vesicles.[40] Lv et al. further observed mixed inverse bicontinuous mesophases.[27] However, it can be found that, until now, the preparation of higher-order morphologies using PICA is all based on RAFT dispersion polymerization. Alternatively, living anionic polymerization (LAP), as the earliest living/controlled polymerization mechanism, allows the large-scale synthesis of the polymer with narrow molecular weight distribution (M_w/M_n), controlled molecular weight (MW), and well-defined compositions and structures.[41−44] Meanwhile, the monomers can be polymerized with a rapid polymerization rate and quantitative monomer conversion (close to 100%). Unfortunately, due to the serious operation, strict conditions, as well as special requirements on the monomers/living species and the limited solvent, there are few works on the heterogeneous LAP PISA system.[45−51]

Motivated by the surging interest in the efficient access to higher-order morphologies, herein, the LAP PICA combining LAP mechanism with the PICA process was attempted using polyisoprene-*b*-polystyrene (PI-*b*-PS)/polystyrene (PS) blends as the research mode. In detail, the macromolecular initiator PI-*b*-PS$^-$Li$^+$ was first synthesized by sequential LAP of isoprene (Is) and styrene (St), then St was cooperatively initiated by macromolecular initiator PI-*b*-PS$^-$Li$^+$ and small molecular initiator *n*-butyllithium (*n*-Bu$^-$Li$^+$) in *n*-heptane, and the LAP PICA process was thus realized (Scheme 1). By modulating the molar ratio [PI-*b*-PS$^-$Li$^+$]/[*n*-Bu$^-$Li$^+$] and solid content, the degree of polymerization (DP_{PS}) and the content of PS homopolymer correspondingly varied. The morphologies such as spheres, worms, jellyfish, vesicles, sponges, and mixed ordered mesophases of *Im*3*m* cubosomes and *p*6*mm* hexosomes were captured and systematically monitored by transmission electron microscopy (TEM), field-emission scanning electron microscopy (FESEM), dynamic light scattering (DLS), and small-angle X-ray scattering (SAXS). Morphological distribution diagrams were constructed to provide guiding principles for the synthesis of desirable morphologies, and the possible formation mechanism was presented.

RESULTS AND DISCUSSION

Preparation of PI-*b*-PS/PS Blends-Based Nano-Objects via LAP PICA. As an extended technique to PISA, PICA is more efficient than PISA in capturing higher-order morphologies.[27,36−40] Aiming to practice LAP PICA process, the living species of PI-*b*-PS$^-$Li$^+$ was first synthesized by sequential LAP of Is and St monomers. The obtained PI-*b*-PS$^-$Li$^+$ was employed as the solvophilic macromolecular initiator in the *n*-heptane solvent, followed by the supplement of small molecular initiator *n*-Bu$^-$Li$^+$. Subsequently, the St monomer was simultaneously initiated by these two initiators, and the core-forming PS block was generated. Finally, the PI-*b*-PS/PS blends-based nano-objects were collected (Scheme 1). In the PICA system, the MW ratio $M_{n,PS}/M_{n,PI}$ in the diblock copolymer PI-*b*-PS, DP_{PS} and content of the PS homopolymer, and the solid content should have an important effect on the morphological evolution of nano-objects. Thus, a series of LAP PICA formulations were performed and investigated in this contribution (Table 1). Specifically, the solid content was fixed as 20% w/w. The DP of the macromolecular initiator PI$^-$Li$^+$ was fixed in the range of 75−95. The $M_{n,PS}/M_{n,PI}$ in the diblock copolymer PI-*b*-PS was designed as 3/1, 4/1, and 6/1. The DP_{PS} and content of the PS homopolymer were modulated by the monomer feed mode and the molar ratio [PI-*b*-PS$^-$Li$^+$]/[*n*-Bu$^-$Li$^+$].

The LAP PICA at two polymerization stages was first manifested by proton nuclear magnetic resonance (^{1}H NMR) and size exclusion chromatography (SEC). As the exemplified ^{1}H NMR spectrum shows in Figure S1, all characteristic proton signals of PI and PS blocks are clearly assigned, and no signals attributed to the double bond on remaining Is or St monomers can be detected, giving reliable evidence that the conversion of each monomer was 100%. By varying the DP_{PS} of the PS homopolymer (designed as 30, 50, and 115) and the MW ratio $M_{n,PS}/M_{n,PI}$ (designed as 3/1, 4/1, and 6/1) in the diblock copolymer PI-*b*-PS, the SEC traces for the LAP PICA system from different formulations are shown in Figures 1 and S2. The symmetrical peaks with narrow M_w/M_n (<1.10) attributed to PI, PI-*b*-PS, and PS can be clearly discriminated, proving that the LAP PICA was performed in a controlled manner in one pot. Thus, the LAP mechanism with the high monomer conversion, narrow M_w/M_n, and controlled MW greatly expanded the scope of the PICA technique.

Effect of DP_{PS} and Content of the PS Homopolymer on the Morphological Evolution of Nano-Objects. As a comparison with PICA, a formulation without the addition of the PS homopolymer was first performed by designing the MW ratio $M_{n,PS}/M_{n,PI}$ in the diblock copolymer PI-*b*-PS as 3/1 (**Entry 1** in Table 1). As shown in Figure 2a, the process was a

https://doi.org/10.1021/acs.macromol.3c00759
Macromolecules 2023, 56, 5743−5753

Table 1. Formulation and Characterization for PI-*b*-PS/PS Blends-Based Nano-Objects with Varied $M_{n,PS}/M_{n,PI}$, [PI-*b*-PS$^-$Li$^+$]/[*n*-Bu$^-$Li$^+$], DP_{PS}, and Contents of the PS Homopolymer[a]

entry	sample[b]	designed [PI-*b*-PS$^-$Li$^+$]/[*n*-Bu$^-$Li$^+$]	designed DP_{PS} of PS homopolymer	designed content of PS homopolymer (%)[c]	PI		PI-*b*-PS/PS blends				morphologies[e]
					$M_{n,PI}$[d]	M_w/M_n[d]	$M_{n,PI\text{-}b\text{-}PS}$[d]	M_w/M_n[d]	$M_{n,PS}$[d]	M_w/M_n[d]	
designed $M_{n,PS}/M_{n,PI}$ = 3/1											
1	PI_{94}-*b*-PS_{188}	1/0	0	0	6400	1.07	26,000	1.05	/	/	sphere and short worm
2	PI_{76}-*b*-PS_{228}/PS_{23}	1/1	30	14	5200	1.05	29,000	1.04	2400	1.05	sphere and short worm
3	PI_{86}-*b*-PS_{193}/PS_{26}	1/3	30	33	5900	1.06	26,000	1.05	2800	1.05	worm and vesicle
4	PI_{80}-*b*-PS_{235}/PS_{31}	1/5	30	45	5500	1.08	30,000	1.05	3300	1.07	oligolamellar vesicle
5	PI_{95}-*b*-PS_{274}/PS_{35}	1/8	30	57	6500	1.08	35,000	1.02	3700	1.16	sponge
6	PI_{91}-*b*-PS_{190}/PS_{49}	1/1	50	25	6200	1.08	26,000	1.04	5100	1.07	worm
7	PI_{85}-*b*-PS_{194}/PS_{44}	1/3	50	50	5800	1.05	26,000	1.04	4600	1.08	vesicle
8	PI_{86}-*b*-PS_{202}/PS_{51}	1/5	50	63	5900	1.07	27,000	1.03	5400	1.07	sponge
9	PI_{79}-*b*-PS_{226}/PS_{62}	1/8	50	72	5400	1.05	29,000	1.03	6500	1.17	sphere
10	PI_{91}-*b*-PS_{200}/PS_{115}	1/1	115	39	6200	1.07	27,000	1.02	12,000	1.02	sphere
11	PI_{91}-*b*-PS_{200}/PS_{115}	1/3	115	67	6200	1.07	27,000	1.01	12,000	1.04	sphere
12	PI_{94}-*b*-PS_{178}/PS_{115}	1/5	115	76	6400	1.08	25,000	1.05	/	/	precipitate
designed $M_{n,PS}/M_{n,PI}$ = 4/1											
13	PI_{86}-*b*-PS_{231}	1/0	50	0	5900	1.09	30,000	1.05	/	/	worm
14	PI_{85}-*b*-PS_{251}/PS_{58}	1/1	50	20	5800	1.06	32,000	1.06	6100	1.04	sphere
15	PI_{82}-*b*-PS_{244}/PS_{49}	1/3	50	42	5600	1.08	31,000	1.06	5100	1.11	sponge
16	PI_{88}-*b*-PS_{250}/PS_{57}	1/5	50	55	6000	1.07	32,000	1.05	5900	1.09	porous vesicle
17	PI_{92}-*b*-PS_{285}/PS_{48}	1/8	50	66	6300	1.06	36,000	1.04	5000	1.17	precipitate
designed $M_{n,PS}/M_{n,PI}$ = 6/1											
18	PI_{95}-*b*-PS_{379}	1/0	50	0	6500	1.06	46,000	1.07	/	/	vesicle
19	PI_{82}-*b*-PS_{340}/PS_{60}	1/1	50	14	5600	1.08	41,000	1.04	6300	1.04	vesicle
20	PI_{84}-*b*-PS_{358}/PS_{59}	1/3	50	33	5700	1.05	43,000	1.04	6200	1.07	sphere and vesicle
21	PI_{92}-*b*-PS_{391}/PS_{49}	1/5	50	45	6300	1.09	47,000	1.04	5100	1.10	porous vesicle

[a]The solid content was fixed as 20% w/w. [b]The subscripts represent the DP of each block, which was calculated according to the SEC and ^{1}H NMR measurements. [c]Content of PS homopolymer (%) is defined as the weight percentage of the PS homopolymer in the total PS block based on the [PI-*b*-PS$^-$Li$^+$]/[*n*-Bu$^-$Li$^+$] value and the monomer feed mode. [d]The M_n and M_w/M_n were obtained by SEC measurement using THF as the eluent and PS as the standard. [e]The morphologies were monitored by TEM measurement.

https://doi.org/10.1021/acs.macromol.3c00759
Macromolecules 2023, 56, 5743−5753

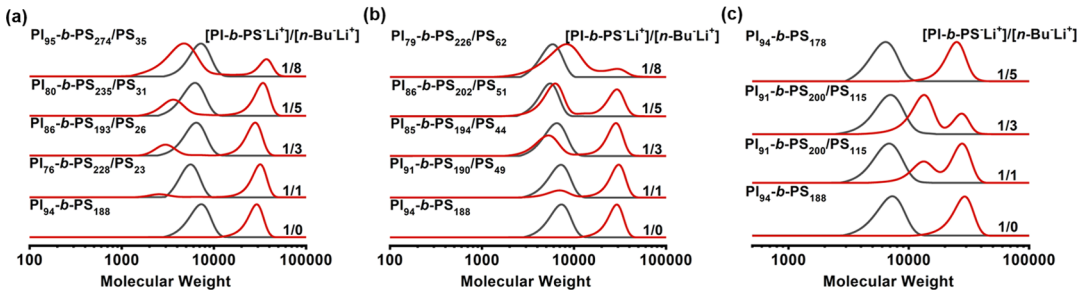

Figure 1. SEC traces for PI (black curves) and the corresponding PI-*b*-PS/PS blends (red curves). The solid content was fixed as 20% w/w. The $M_{n,PS}/M_{n,PI}$ in the diblock copolymer PI-*b*-PS was fixed as 3/1. The DP_{PS} was designed as (a) 30, (b) 50, and (c) 115, respectively. The content of the PS homopolymer was modulated by the molar ratio [PI-*b*-PS$^-$Li$^+$]/[*n*-Bu$^-$Li$^+$] = 1/0, 1/1, 1/3, 1/5, and 1/8.

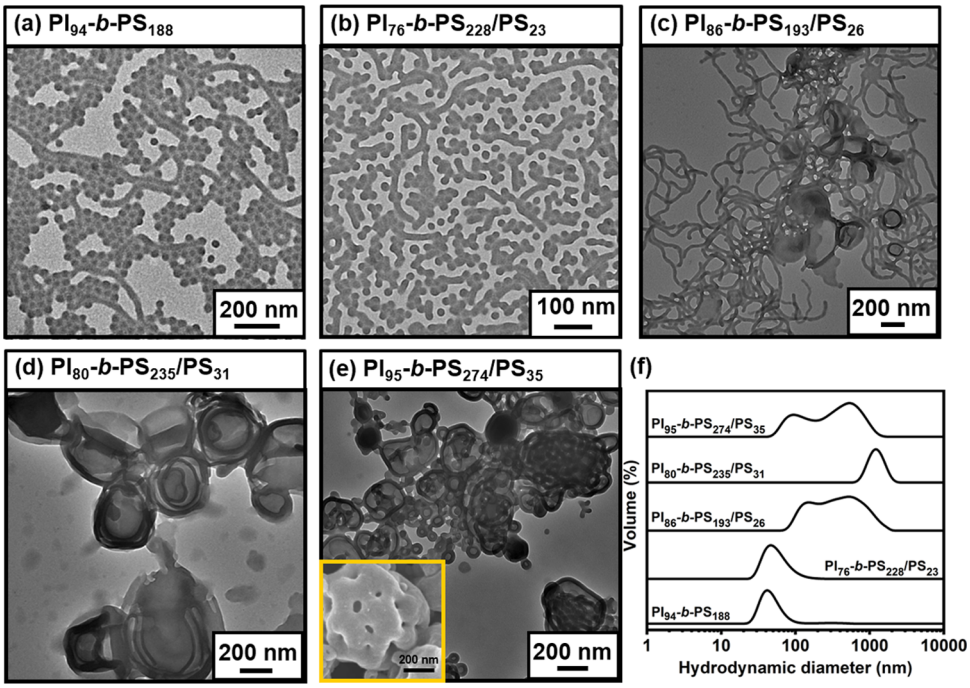

Figure 2. TEM and FESEM images of PI-*b*-PS/PS nano-objects (diluted to 0.01−0.3% w/w dispersions) formed in PISA or LAP PICA process using the macromolecular initiator PI$^-$Li$^+$ with DP in the range of 75−95, $M_{n,PS}/M_{n,PI}$ of 3/1 in the diblock copolymer, solid content of 20% w/w, DP_{PS} of approximately 30, and different [PI-*b*-PS$^-$Li$^+$]/[*n*-Bu$^-$Li$^+$]: (a) 1/0, (b) 1/1, (c) 1/3, (d) 1/5, and (e) 1/8. (f) DLS results of the corresponding nano-objects (diluted into 0.01−0.3% w/w dispersions).

typical PISA system, and the mixture of spheres and short worms with an average diameter of 43 ± 19 nm can be observed, which was consistent with the previously demonstrated work in our group.[50] Alternatively, once the PS homopolymer was introduced and the LAP PICA process was realized, the morphologies can be derived in a broad window as illustrated in the following section.

When the DP_{PS} was designed as about 30, the morphological evolution is shown in Figure 2 by modulating the molar ratio [PI-*b*-PS$^-$Li$^+$]/[*n*-Bu$^-$Li$^+$]. When [PI-*b*-PS$^-$Li$^+$]/[*n*-Bu$^-$Li$^+$] was designed as 1/1, the content of PS homopolymer was 17%, and the PICA system remained a mixture of spheres and short worms with an average diameter of around 50 ± 22 nm (Figure 2b). When [PI-*b*-PS$^-$Li$^+$]/[*n*-Bu$^-$Li$^+$] was decreased to 1/3 and the content of the PS homopolymer was increased to 33%, a mixture of worms and vesicles was captured (Figure 2c). Correspondingly, the DLS curve showed a bimodal distribution (Figure 2f). Continuously, the curvature energy induced the formation of large 'vesicles within vesicles' (*a.k.a.*, oligolamellar vesicles, OLVs[52]) when [PI-*b*-PS$^-$Li$^+$]/[*n*-Bu$^-$Li$^+$] was decreased to 1/5 and the content of PS homopolymer was increased to 45% (Figure 2d). In this case, the DLS curve showed a unimodal peak with a large size around 1281 ± 569 nm (Figure 2f). When [PI-*b*-PS$^-$Li$^+$]/[*n*-Bu$^-$Li$^+$] was further decreased to 1/8 and the content of PS homopolymer was increased to 56% (Figure 2e), the TEM and FESEM measurements consistently indicated that the sponge structures with a porous rough surface were generated.

When the DP_{PS} was designed at approximately 50, the morphologies of the nano-objects with different [PI-*b*-PS$^-$Li$^+$]/[*n*-Bu$^-$Li$^+$] underwent a sequence of evolution from spheres ([PI-*b*-PS$^-$Li$^+$]/[*n*-Bu$^-$Li$^+$] = 1/0, Figure 3a), worms ([PI-*b*-PS$^-$Li$^+$]/[*n*-Bu$^-$Li$^+$] = 1/1, Figure 3b), vesicles ([PI-*b*-PS$^-$Li$^+$]/[*n*-Bu$^-$Li$^+$] = 1/3, Figure 3c), sponges ([PI-*b*-PS$^-$Li$^+$]/[*n*-Bu$^-$Li$^+$] = 1/5, Figure 3d), and back to spheres ([PI-*b*-PS$^-$Li$^+$]/[*n*-Bu$^-$Li$^+$] = 1/8, Figure 3e). DLS curves in Figure 3f showed consistent results with those from the TEM measurement. Specifically, the hydrodynamic diameter of the spheres obtained with [PI-*b*-PS$^-$Li$^+$]/[*n*-Bu$^-$Li$^+$] = 1/8 (396 ± 141 nm) (Figure 3e) was obviously larger than that with [PI-*b*-

https://doi.org/10.1021/acs.macromol.3c00759
Macromolecules 2023, 56, 5743−5753

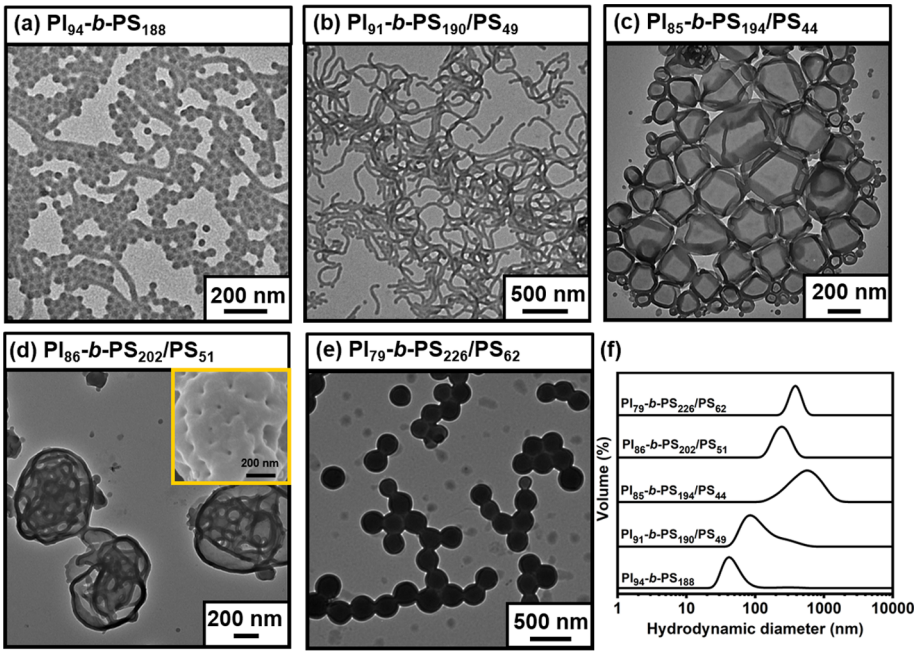

Figure 3. TEM and FESEM images of PI-*b*-PS/PS nano-objects (diluted into 0.01−0.3% w/w dispersions) formed in the PISA or LAP PICA process using the macromolecular initiator PI^-Li^+ with DP in the range of 75−95, $M_{n,PS}/M_{n,PI}$ of 3/1 in the diblock copolymer, solid content of 20% w/w, DP_{PS} of approximately 50, and different [PI-*b*-PS^-Li^+]/[*n*-Bu^-Li^+]: (a) 1/0, (b) 1/1, (c) 1/3, (d) 1/5, and (e) 1/8. (f) DLS results of the corresponding nano-objects (diluted into 0.01−0.3% w/w dispersions).

PS^-Li^+]/[*n*-Bu^-Li^+] = 1/0 (43 ± 19 nm) (Figure 3a). In these formulations, besides the screened phenomenon of lower-order morphologies to higher-order morphologies as a decreasing [PI-*b*-PS^-Li^+]/[*n*-Bu^-Li^+] value, a morphological transition from sponges to spheres was also observed. Furthermore, when the DP_{PS} was designed at about 115 and [PI-*b*-PS^-Li^+]/[*n*-Bu^-Li^+] was designed as 1/1 and 1/3, the spheres with 142 ± 50 and 459 ± 204 nm were prepared (Figure 4b,c,d), which again had larger sizes than those obtained in the LAP PISA system (Figure 4a,d). However, when the [PI-*b*-PS^-Li^+]/[*n*-Bu^-Li^+] was decreased as 1/5, precipitation was observed in the LAP PICA system. The reason might be attributed to the higher content of PS homopolymer (76%), which cannot be stabilized by the solvophilic PI block.

Furthermore, in order to evaluate the versatility of LAP PICA, a series of LAP PICA systems were performed by varying $M_{n,PS}/M_{n,PI}$ and [PI-*b*-PS^-Li^+]/[*n*-Bu^-Li^+], and fixing DP_{PS} as about 50 (Figure S2). The PISA system targeting at $M_{n,PS}/M_{n,PI}$ = 4/1 (**Entry 13** in Table 1) and 6/1 (**Entry 18** in Table 1) in the diblock copolymer with the solid content as 20% w/w produced morphologies of worms (Figure 5a) and vesicles (Figure 5e), respectively. When targeted $M_{n,PS}/M_{n,PI}$ was designed as 4/1, morphological transformations from worms ([PI-*b*-PS^-Li^+]/[*n*-Bu^-Li^+] = 1/0, Figure 5a) to spheres ([PI-*b*-PS^-Li^+]/[*n*-Bu^-Li^+] = 1/1, Figure 5b), irregular sponges ([PI-*b*-PS^-Li^+]/[*n*-Bu^-Li^+] = 1/3, Figure 5c), and porous vesicles ([PI-*b*-PS^-Li^+]/[*n*-Bu^-Li^+] = 1/5, Figure 5d) were observed. Continuously, when the [PI-*b*-PS^-Li^+]/[*n*-Bu^-Li^+] was decreased to 1/8, the precipitation was generated due to the relatively higher content of the PS homopolymer (66%) and, correspondingly, the reduced stability by the solvophilic PI block. When targeted $M_{n,PS}/M_{n,PI}$ was increased to 6/1, with the increase of the PS homopolymer content, the morphologies from thin-walled vesicles ([PI-*b*-PS^-Li^+]/[*n*-Bu^-Li^+] = 1/0, Figure 5e) to thick-walled vesicles ([PI-*b*-PS^-Li^+]/[*n*-Bu^-Li^+] = 1/1, Figure 5f), the mixture of thick-walled vesicles and spheres ([PI-*b*-PS^-Li^+]/[*n*-Bu^-Li^+] = 1/3, Figure 5g), and porous vesicles ([PI-*b*-PS^-Li^+]/[*n*-Bu^-Li^+] = 1/5, Figure 5h) were captured. DLS curves in Figure S3 show consistent results with those from the TEM measurement.

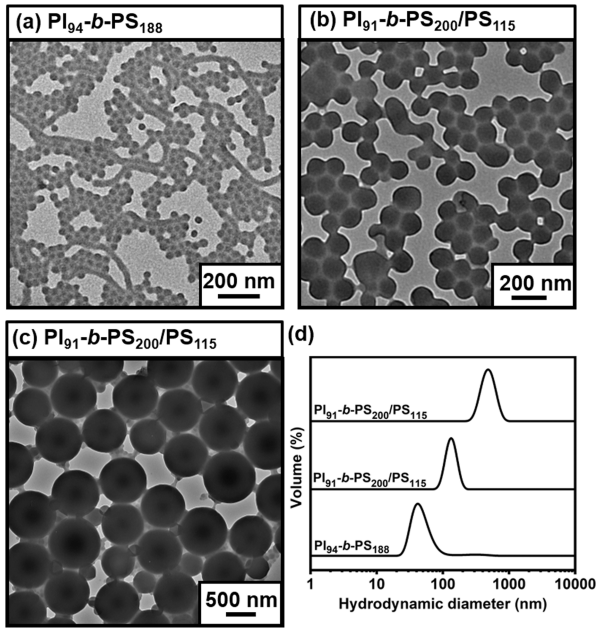

Figure 4. TEM images of PI-*b*-PS/PS nano-objects (diluted into 0.01−0.3% w/w dispersions) formed in the PISA or LAP PICA process using the macromolecular initiator PI^-Li^+ with DPs in the range of 75−95, $M_{n,PS}/M_{n,PI}$ of 3/1 in the diblock copolymer, solid content of 20% w/w, DP_{PS} of approximately 115, and different [PI-*b*-PS^-Li^+]/[*n*-Bu^-Li^+]: (a) 1/0, (b) 1/1, and (c) 1/3. (d) DLS results of the corresponding nano-objects (diluted into 0.01−0.3% w/w dispersions).

https://doi.org/10.1021/acs.macromol.3c00759
Macromolecules 2023, 56, 5743−5753

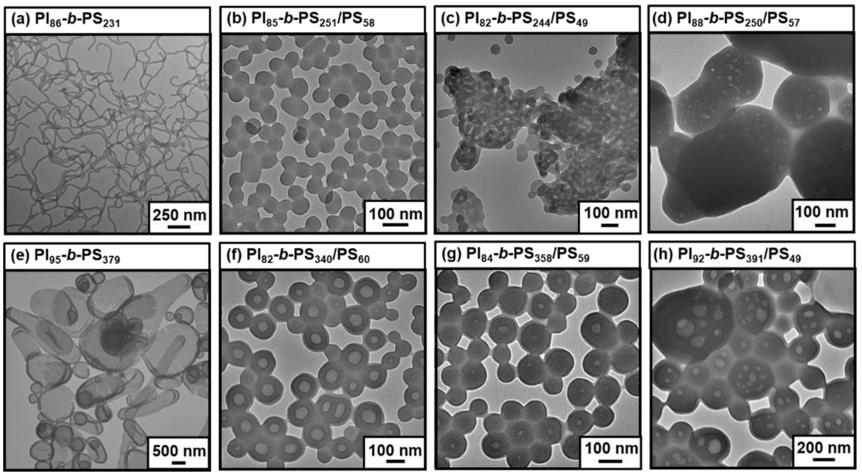

Figure 5. TEM images of PI-*b*-PS/PS nano-objects (diluted into 0.01−0.3% w/w dispersions) formed in PISA or LAP PICA process using the macromolecular initiator PI^-Li^+ with DP in the range of 75−95, $M_{n,PS}/M_{n,PI}$ of 4/1 (a−d), and 6/1 (e−h) in the diblock copolymer, solid content of 20% w/w, DP_{PS} of approximately 50, and different $[PI\text{-}b\text{-}PS^-Li^+]/[n\text{-}Bu^-Li^+]$: (a, e) 1/0, (b, f) 1/1, (c, g) 1/3, and (d, h) 1/5.

Table 2. Formulation and Characterization for PI-b-PS/PS Blends-Based Nano-Objects with Varied Solid Contents (20, 30, and 40% w/w), DP_{PS}, and Contents of PS Homopolymer and Fixed $M_{n,PS}/M_{n,PI}$ = 3/1 and $[PI\text{-}b\text{-}PS^-Li^+]/[n\text{-}Bu^-Li^+]$ = 1/3

entry	sample[a]	solid content (% w/w)	designed content of PS homopolymer (%)[b]	PI		PI-*b*-PS/PS blends				morphologies[d]
				$M_{n,PI}$[c]	M_w/M_n[c]	$M_{n,PI\text{-}b\text{-}PS}$[c]	M_w/M_n[c]	$M_{n,PS}$[c]	M_w/M_n[c]	
1	PI_{86}-*b*-PS_{193}/PS_{26}	20	33	5900	1.06	26,000	1.04	2800	1.05	mixture of worm and vesicle
2	PI_{94}-*b*-PS_{188}/PS_{23}	30	33	6400	1.07	26,000	1.05	2400	1.04	mixture of sphere, worm and jellyfish
3	PI_{85}-*b*-PS_{190}/PS_{25}	40	33	5800	1.07	25,000	1.04	2600	1.07	
4	PI_{85}-*b*-PS_{194}/PS_{44}	20	50	5800	1.08	26,000	1.04	4600	1.08	vesicle
5	PI_{79}-*b*-PS_{207}/PS_{46}	30	50	5400	1.08	27,000	1.05	4800	1.08	vesicle
6	PI_{83}-*b*-PS_{204}/PS_{43}	40	50	5700	1.07	27,000	1.04	4500	1.05	inverse bicontinuous phases
7	PI_{91}-*b*-PS_{205}/PS_{115}	20	67	6200	1.08	27,000	1.01	12,000	1.04	sphere
8	PI_{94}-*b*-PS_{198}/PS_{115}	30	67	6400	1.07	27,000	1.02	12,000	1.04	porous vesicle
9	PI_{97}-*b*-PS_{200}/PS_{115}	40	67	6600	1.06	28,000	1.02	12,000	1.04	porous vesicle

[a]The subscripts represented the DP of each block, which was calculated according to the SEC and ^{1}H NMR measurements. [b]Content of PS homopolymer (%) is defined as the weight percentage of the PS homopolymer in the total PS block based on the $[PI\text{-}b\text{-}PS^-Li^+]/[n\text{-}Bu^-Li^+]$ value and the monomer feed mode. [c]The M_n and M_w/M_n were obtained by SEC measurement using THF as the eluent and PS as the standard. [d]The morphologies were monitored by TEM measurement.

These results indicated that efficient morphological transformation via LAP PICA could also begins with intermediate morphologies of worms or vesicles. Additionally, except for the formulations with a high MW or content of PS homopolymer (**Entry 12 and 17** in Table 1), it should be noted that no precipitate can be discriminated in most LAP PICA systems, although the PS homopolymer was insoluble in *n*-heptane.

Effect of Solid Contents on Morphological Evolution of Nano-Objects. The solid content in the self-assembly process is also an important factor. Higher solid content has been demonstrated to facilitate the formation of higher-order morphologies.[25,29] To explore its feasibility in LAP PICA, the formulations with different solid contents ranging from 20 to 40% w/w and targeted DP_{PS} at 30 (**Entries 1−3** in Table 2), 50 (**Entries 4−6** in Table 2). and 115 (**Entries 7−9** in Table 2) were performed. As expected, the PI and PI-*b*-PS/PS blends with narrow M_w/M_n (<1.10) and controlled MWs were successfully synthesized with high monomer conversion (close to 100%) (Figure S4). The TEM and FESEM micrographs are shown in Figure 6, and the corresponding DLS curves are depicted in Figure S5.

When the DP_{PS} was designed as around 30, higher-order morphologies were not captured as expected, but only a mixture of spheres, worms, and jellyfish was observed when the solid contents was increased from 20 to 30% or 40% w/w (Figure 6a,d,g). When the designed DP_{PS} was increased to 50, thick-walled vesicles with internal spheres were obtained in the system with 30% w/w (Figure 6e). Surprisingly, the structure of the inverse bicontinuous mesophases was accessed at a solid content as high as 40% w/w (Figure 6h). When the DP_{PS} was designed as 115, a morphological transition from large-size spheres (Figure 6c) to porous vesicles (Figure 6f,i) was observed as the solid contents increased from 20 to 30% and 40%. By summarizing the results, we can find that the higher solid content and higher DP_{PS} (50 and 115) contributed to the higher-order morphologies. The reason can be attributed to the effective inelastic collisions, fusion, and chain rearrangement between nano-objects under high solid content, as well as the synergistic effect enhanced by the insolubility of the PS homopolymer.

SAXS Studies on PI-*b*-PS/PS Blends-Based Nano-Objects. SAXS technique, as an in situ method for assessing the morphologies of nano-objects, was used to study PI-*b*-PS/

https://doi.org/10.1021/acs.macromol.3c00759
Macromolecules 2023, 56, 5743−5753

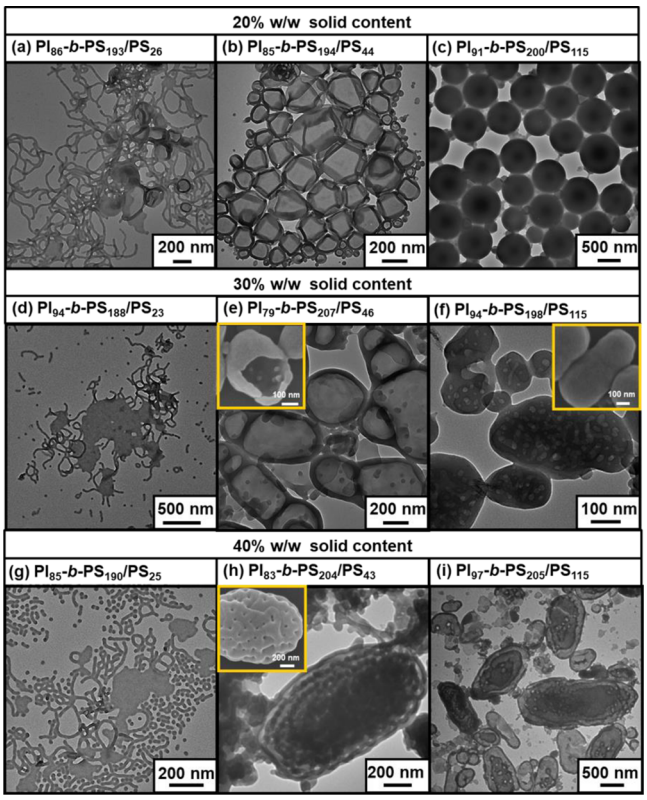

Figure 6. TEM and FESEM images of PI-*b*-PS/PS nano-objects (diluted into 0.01−0.3% w/w dispersions) formed in the LAP PICA process using the macromolecular initiator $PI^{-}Li^{+}$ with DP in the range of 75−95, $M_{n,PS}/M_{n,PI}$ of 3/1, DP_{PS} of approximately 30, 50, and 115, and different solid contents: (a−c) 20% w/w, (d−f) 30% w/w, and (g−i) 40% w/w.

PS blends-based nano-objects (Figure 7). The scattering patterns obtained for nano-objects from PI_{94}-*b*-PS_{188}, PI_{91}-*b*-PS_{190}/PS_{49}, and PI_{85}-*b*-PS_{194}/PS_{44} (**Entries 1**, **6**, and **7** in Table 1) exhibit a gradient change of 0, −1, and −2 in the low q section (Figure 7a), which are in fairly good agreement with the morphologies of spheres, worms, and vesicles in the literature[53,54] and in our TEM images. The SAXS pattern of spheres (red curves in Figure 7a) slightly deviated from a zero slope at low q (less than 0.01 A^{-1}), suggesting the presence of a small amount of dimer and trimer or even traces of worms,[55] which was also verified by the corresponding TEM image.

Using the SAXS technique, the nano-objects with complex internal structures were also elucidated. For the spongy nano-objects from PI_{86}-*b*-PS_{202}/PS_{51} (Figure 3d, Entry 8 in Table 1), less resolved signals were captured in the SAXS profile (Figure 7b). This was because the sponges, generally considered as a "melted" cubic phase, were less regular than cubosomes, despite having bicontinuous channels.[29] For the inverse bicontinuous mesophases from PI_{83}-*b*-PS_{204}/PS_{43} (Figure 6h), the corresponding SAXS showed three weak signals with a q^2 ratio of 2:4:6 (Figure 7c), which were indexed to the (110), (200), and (211) reflections of the primitive cubic lattice (*Im*3*m*) of cubosomes.[56] The lattice constant (a) was calculated to be 48 nm. Noteworthily, another defined peak assigned to (10) reflection of the *p6mm* space group accompanied by a hardly resolvable (11) reflection is also found in Figure 7c, which narrowly indicated the presence of hexosomes. In principle, the specific structure of mixed *Im*3*m* cubosomes and *p6mm* hexosomes could not be defined based on such ambiguous peaks in Figure 7c. Alternatively, these assignments can be affirmed by TEM images exhibiting concentric hoops (characteristic of *p6mm* hexosomes[29,57]) and bicontinuous channels with porous ellipsoidal surfaces (characteristic of *Im*3*m* cubosomes[58−60]) (TEM and FESEM in Figure 6h).

Explanation and Analysis on Morphological Evolution in LAP PICA. The above results confirmed that LAP PICA can indeed generate higher-order morphologies more effectively than LAP PISA. To further understand the effect of factors on the morphological evolution of nano-objects in the LAP PICA process, a detailed morphological distribution diagram was depicted based on the relationship between DP_{PS} and the content of the PS homopolymer (Figure 8a), as well as DP_{PS} and solid contents (Figure 8b). As shown in Figure 8a, maintaining DP_{PS} below 50 and increasing the content of the PS homopolymer promoted the morphological transformation to higher-order (such as sponges), which provided solid evidence that the high content of the PS homopolymer had a profound impact in boosting morphological transition. However, when the DP_{PS} was above 50, no obvious change could be discriminated and the spheres were always collected with the increase in the content of the PS homopolymer. Alternatively, in Figure 8b, it can be observed that the higher solid content and DP_{PS} lead to higher-order morphologies, and appropriate solid content and DP_{PS} contributed to the inverse bicontinuous mesophase with a narrow window. In brief, these two morphological distribution diagrams provide resultful guidance for the selective preparation of nano-objects with specific morphologies. The feasible mechanisms of these phenomena are elaborated below.

First, under the circumstance of DP_{PS} around 30 and solid content of 20% w/w, the morphologies underwent a series of

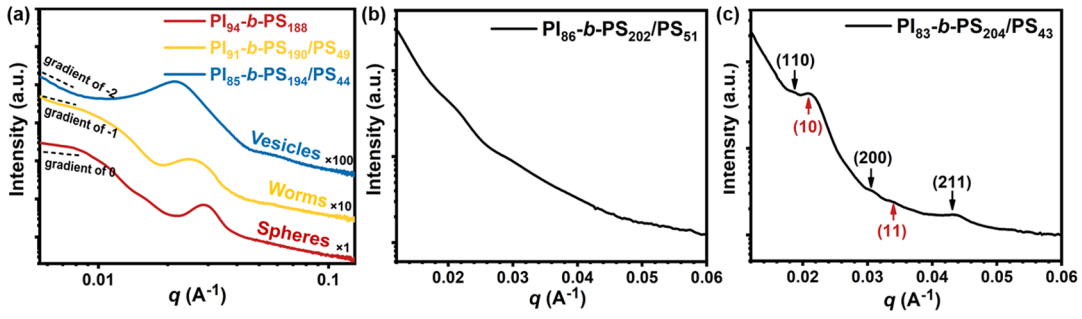

Figure 7. SAXS profiles of PI-*b*-PS/PS nano-objects with representative morphologies: (a) spheres, worms, and vesicles; (b) sponges; and (c) mixed *Im*3*m* cubosomes and *p6mm* hexosomes. (Note: q in red color is for *p6mm* and q in black color is for *Im*3*m* in (c) images.)

https://doi.org/10.1021/acs.macromol.3c00759
Macromolecules 2023, 56, 5743−5753

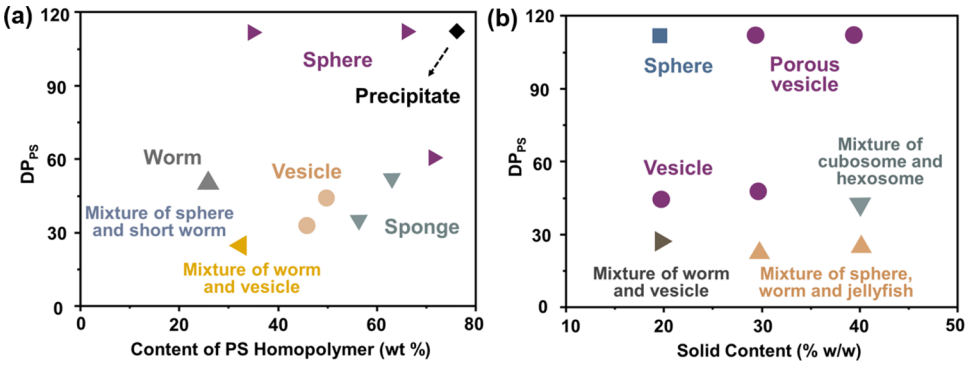

Figure 8. Morphological distribution diagram based on the variation: (a) DP_{PS} and content of the PS homopolymer with a fixed solid content of 20% w/w, and (b) DP_{PS} and solid contents with fixed [PI-*b*-PS$^-$Li$^+$]/[*n*-Bu$^-$Li$^+$] = 1/3. Note: For the simplicity of this diagram, oligolamellar vesicles, unilamellar vesicles, and porous vesicles were all labeled as the vesicle phase.

Scheme 2. Schematic Illustration of the Morphological Evolution: (a) from Spheres (I) to Worms (II), Vesicles (III), Sponges (IV, V), and Spheres (VI) with a Solid Content of 20% w/w; (b) from Spheres (VII) to Porous Vesicles (VII) with a Solid Contents of 30 and 40% w/w via LAP PICA

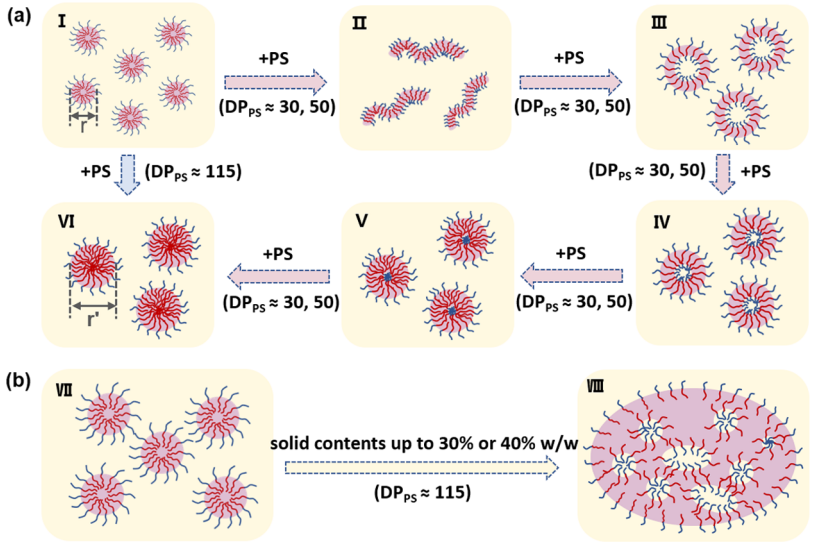

Note: the red curves represent the core-forming block and the blue curves represent the solvophilic PI block.

transitions from lower-order [mixture of spheres (I) and worms (II); mixture of worms and vesicles (III)] to higher-order [vesicles or sponges (IV)] as the content of the PS homopolymer was gradually increased (Figure 2 and Scheme 2a). This phenomenon can be explained by the variation of packing parameter $P = v/a_0l_c$, which is a result of a force balance involving the stretching of the core-forming blocks in the core, the interfacial tension between the core and the solvent, and the intercorona interactions.[61,62] Herein, when the PS homopolymer was added, the volume of core-forming PS block (v) increases, while the chain extension of the solvophobic PS block (l_c) decreases. Hence, the P value increases, manifesting as the morphological transition from spheres to higher-order morphologies.

Second, when DP_{PS} was around 50 and the solid content was fixed as 20% w/w, the morphological evolution conformed to the expected transformation from spheres (I) to worms (II), vesicles (III), and sponges (IV) with the increase of the content of the PS homopolymer (Figure 3 and Scheme 2a). However, with the continued addition of the PS homopolymer, the solvophilic PI block was insufficient to support further expansion of the sponges. At this moment, the optimum state of thermodynamic equilibrium was to squeeze the solvent in the sponges outward, so that more solvophobic PS homopolymers can be accommodated inside. As a consequence, the core-forming section became denser and denser [from (IV) to (V)], and a kind of flip-flop mechanism subsequently took place.[14] Finally, the sponge transformed into thermodynamically stable spheres [from (V) to (VI)].

Third, when DP_{PS} was increased to around 115 and the solid content was fixed as 20% w/w, the PS homopolymer stabilized by the block copolymer PI-*b*-PS favored aggregating near the core due to the decreased solubility driven by phase separation. Thus, the stretching extent of the PS block in the block copolymer was significantly lowered, and the entropy penalty associated with chain stretching was reduced. Therefore, the sphere which was conducive to minimizing the free energy of the interface was preferred [from (I) to (VI), Scheme 2a]. Alternatively, under a higher solid contents of 30 and 40% w/w, the sphere (VII) can even evolve as a porous vesicle (VII) due to the enhanced inelastic collisions, fusion, and chain rearrangement between nano-objects, as well as the remarkable

https://doi.org/10.1021/acs.macromol.3c00759
Macromolecules 2023, 56, 5743−5753

cooperative-effect of the PS homopolymer with high DP_{PS} (Scheme 2b).

Additionally, unlike the typical PISA process,[50] the LAP PICA process can adjust the size of the sphere in a wide range just by modulating the DP_{PS} and the content of the PS homopolymer. In a typical PISA process, when the DP of the solvophobic PS block increased, the volume of the core-forming block (v) increased, which resulted in less curved interfaces. Thus, the PS blocks had to rearrange to reduce the entropy penalty associated with chain stretching, leading to a morphological transition from spheres to worms or vesicles without being able to regulate the size of spheres. However, different from the PISA process, the added PS homopolymer in the LAP PICA process preferred to aggregate near the core region,[36] making the solvophobic PS block in the original block copolymer not to extend as much as that in the absence of the PS homopolymer. The free energy was reduced, and the sphere that was most conducive to free energy could be obtained in a broad window. Thus, it was ready to understand that the size of the finally derived spheres (VI) was larger than the original ones (I) because of the filling of the more PS homopolymer (Scheme 2a). In short, the PICA showed great superiority in tuning the size of spheres, which would greatly expand the utility of spherical nano-objects in biomedical applications,[63,64] Pickering emulsifiers,[65] filler for composites,[66] and so on.

CONCLUSIONS

In summary, LAP PICA of PI-*b*-PS/PS has been successfully exploited by varying the DP_{PS} and content of PS homopolymer and the solid content. As these factors were modulated, the morphological transition from spheres to worms, jellyfish, vesicles, sponges, and ordered mesophases of *Im*3*m* cubosomes and *p*6*mm* hexosomes indicated the efficient access to complete morphological range via LAP PICA. Besides, PICA showed great superiority in tuning the size of spheres. The morphological distribution diagrams were depicted to unveil the effect of DP_{PS} and content of the PS homopolymer and the solid content on the transformation of morphologies and provide guiding principles for the tailored synthesis of polymeric nano-objects with a variety of morphologies. The relevant mechanism of morphological transition in LAP PICA was put forward. It is believed that the facile LAP PICA system will greatly expand the scope of PICA and exhibit promising applications in mechanical metamaterials, nanonetwork thermosets, and many other fields.

ASSOCIATED CONTENT

Supporting Information

The Supporting Information is available free of charge at https://pubs.acs.org/doi/10.1021/acs.macromol.3c00759.

Experimental section; characterization section; ^{1}H NMR spectra for representative crude PI and PI-*b*-PS/PS blends; SEC traces for PI and the corresponding PI-*b*-PS/PS blends with $M_{n,PS}/M_{n,PI}$ = 4/1 or 6/1 and different [PI-*b*-PS$^-$Li$^+$]/[*n*-Bu$^-$Li$^+$]; DLS results of nano-objects with $M_{n,PS}/M_{n,PI}$ = 4/1 or 6/1 and different [PI-*b*-PS$^-$Li$^+$]/[*n*-Bu$^-$Li$^+$]; SEC traces for PI and the corresponding PI-*b*-PS/PS blends with $M_{n,PS}/M_{n,PI}$ = 3/1 and different DP_{PS} and solid contents; and DLS results of nano-objects with $M_{n,PS}/M_{n,PI}$ = 3/1 or 6/1 and different DP_{PS} and solid contents (PDF)

AUTHOR INFORMATION

Corresponding Author

Guowei Wang − *State Key Laboratory of Molecular Engineering of Polymers, Department of Macromolecular Science, Fudan University, Shanghai 200433, China;* orcid.org/0000-0003-2595-8269; Email: gwwang@fudan.edu.cn

Authors

Jingwei Zhang − *State Key Laboratory of Molecular Engineering of Polymers, Department of Macromolecular Science, Fudan University, Shanghai 200433, China*

Peng Zhou − *State Key Laboratory of Molecular Engineering of Polymers, Department of Macromolecular Science, Fudan University, Shanghai 200433, China*

Boyang Shi − *State Key Laboratory of Molecular Engineering of Polymers, Department of Macromolecular Science, Fudan University, Shanghai 200433, China*

Penghan Li − *State Key Laboratory of Molecular Engineering of Polymers, Department of Macromolecular Science, Fudan University, Shanghai 200433, China*

Complete contact information is available at: https://pubs.acs.org/10.1021/acs.macromol.3c00759

Notes

The authors declare no competing financial interest.

ACKNOWLEDGMENTS

This work was supported by the National Natural Science Foundation of China (21774022 and 22271058).

REFERENCES

(1) Wang, Z.; Van Oers, M. C. M.; Rutjes, F. P. J. T.; Van Hest, J. C. M. Polymersome Colloidosomes for Enzyme Catalysis in a Biphasic System. *Angew. Chem., Int. Ed.* **2012**, *51*, 10746−10750.

(2) Holder, S. J.; Sommerdijk, N. New micellar morphologies from amphiphilic block copolymers: disks, toroids and bicontinuous micelles. *Polym. Chem.* **2011**, *2*, 1018−1028.

(3) Blanazs, A.; Armes, S. P.; Ryan, A. J. Self-Assembled Block Copolymer Aggregates: From Micelles to Vesicles and their Biological Applications. *Macromol. Rapid Commun.* **2009**, *30*, 267−277.

(4) Rodriguez-Hernandez, J.; Checot, F.; Gnanou, Y.; Lecommandoux, S. Toward 'smart' nano-objects by self-assembly of block copolymers in solution. *Prog. Polym. Sci.* **2005**, *30*, 691−724.

(5) Tritschler, U.; Pearce, S.; Gwyther, J.; Whittell, G. R.; Manners, I. 50th Anniversary Perspective: Functional Nanoparticles from the Solution Self-Assembly of Block Copolymers. *Macromolecules* **2017**, *50*, 3439−3463.

(6) Jia, L.; Zhao, G.; Shi, W.; Coombs, N.; Gourevich, I.; Walker, G. C.; Guerin, G.; Manners, I.; Winnik, M. A. A design strategy for the hierarchical fabrication of colloidal hybrid mesostructures. *Nat. Commun.* **2014**, *5*, 3882.

(7) Mai, Y.; Eisenberg, A. Self-assembly of block copolymers. *Chem. Soc. Rev.* **2012**, *41*, 5969−5985.

(8) Charleux, B.; Delaittre, G.; Rieger, J.; D'Agosto, F. Polymerization-Induced Self-Assembly: From Soluble Macromolecules to Block Copolymer Nano-Objects in One Step. *Macromolecules* **2012**, *45*, 6753−6765.

(9) Wang, X.; An, Z. New Insights into RAFT Dispersion Polymerization-Induced Self-Assembly: From Monomer Library, Morphological Control, and Stability to Driving Forces. *Macromol. Rapid Commun.* **2019**, *40*, No. 1800325.

(10) Rieger, J. Guidelines for the Synthesis of Block Copolymer Particles of Various Morphologies by RAFT Dispersion Polymerization. *Macromol. Rapid Commun.* **2015**, *36*, 1458−1471.

(11) Canning, S. L.; Smith, G. N.; Armes, S. P. A Critical Appraisal of RAFT-Mediated Polymerization-Induced Self Assembly. *Macromolecules* **2016**, *49*, 1985−2001.
(12) Yeow, J.; Boyer, C. Photoinitiated Polymerization-Induced Self-Assembly (Photo-PISA): New Insights and Opportunities. *Adv. Sci.* **2017**, *4*, No. 1700137.
(13) Penfold, N. J. W.; Yeow, J.; Boyer, C.; Armes, S. P. Emerging Trends in Polymerization-Induced Self-Assembly. *ACS Macro Lett.* **2019**, *8*, 1029−1054.
(14) Israelachvili, J. N. *Intermolecular and surface forces*, 3rd ed.; Elsevier: Amsterdam, 2011; pp 536−539.
(15) Zhu, C.; Nicolas, J. (Bio)degradable and Biocompatible Nano-Objects from Polymerization-Induced and Crystallization-Driven Self-Assembly. *Biomacromolecules* **2022**, *23*, 3043−3080.
(16) Liu, J.; Wu, W. J.; Sun, X. L.; Qian, Q. R.; Xiao, L. R. Degradable polymeric nanomaterials with a high solid content and multiple morphologies by polymerization-induced self-assembly. *Chem. Commun.* **2022**, *58*, 3182−3185.
(17) Lv, F.; An, Z.; Wu, P. What Determines the Formation of Block Copolymer Nanotubes? *Macromolecules* **2019**, *53*, 367−373.
(18) Li, C.; Zhao, W.; He, J.; Zhang, Y.; Zhang, W. Single-Step Expeditious Synthesis of Diblock Copolymers with Different Morphologies by Lewis Pair Polymerization-Induced Self-Assembly. *Angew. Chem., Int. Ed.* **2022**, *134*, No. e202202448.
(19) Damsongsang, P.; Hoven, V. P.; Yusa, S.-I. Core-functionalized nanoaggregates: preparation via polymerization-induced self-assembly and their applications. *New J. Chem.* **2021**, *45*, 12776−12791.
(20) Varlas, S.; Foster, J. C.; Georgiou, P. G.; Keogh, R.; Husband, J. T.; Williams, D. S.; O'Reilly, R. K. Tuning the membrane permeability of polymersome nanoreactors developed by aqueous emulsion polymerization-induced self-assembly. *Nanoscale* **2019**, *11*, 12643−12654.
(21) Zhang, W.-J.; Hong, C.-Y.; Pan, C.-Y. Polymerization-Induced Self-Assembly of Functionalized Block Copolymer Nanoparticles and Their Application in Drug Delivery. *Macromol. Rapid Commun.* **2019**, *40*, No. 1800279.
(22) Chen, M.; Zhang, W.-G.; Li, J.-W.; Hong, C.-Y.; Zhang, W.-J.; You, Y.-Z. Preparation of pH- and reductive-responsive prodrug nanoparticles via polymerization-induced self-assembly. *Sci. China: Chem.* **2018**, *61*, 1159−1166.
(23) Zhang, W. J.; Hong, C. Y.; Pan, C. Y. Formation of Hexagonally Packed Hollow Hoops and Morphology Transition in RAFT Ethanol Dispersion Polymerization. *Macromol. Rapid Commun.* **2015**, *36*, 1428−1436.
(24) Yang, P.; Ning, Y.; Neal, T. J.; Jones, E. R.; Parker, B. R.; Armes, S. P. Block copolymer microparticles comprising inverse bicontinuous phases prepared via polymerization-induced self-assembly. *Chem. Sci.* **2019**, *10*, 4200−4208.
(25) Lv, F.; An, Z.; Wu, P. Scalable preparation of alternating block copolymer particles with inverse bicontinuous mesophases. *Nat. Commun.* **2019**, *10*, 1397.
(26) Luo, X.; An, Z. Polymerization-Induced Self-Assembly for the Synthesis of Poly(N,N-dimethylacrylamide)-b-Poly(4-tert-butoxystyrene) Particles with Inverse Bicontinuous Phases. *Macromol. Rapid Commun.* **2020**, *41*, No. e2000209.
(27) Lv, F.; An, Z.; Wu, P. Efficient Access to Inverse Bicontinuous Mesophases via Polymerization-Induced Cooperative Assembly. *CCS Chem.* **2021**, *3*, 2211−2222.
(28) Luo, X.; An, Z. Polymerization-Induced Self-Assembly for the Preparation of Poly(N,N-dimethylacrylamide)-b-Poly(4-tert-butoxystyrene-co-pentafluorostyrene) Particles with Inverse Bicontinuous Phases. *Chin. J. Chem.* **2021**, *39*, 1819−1824.
(29) Fan, B.; Wan, J.; Zhai, J.; Chen, X.; Thang, S. H. Triggered Degradable Colloidal Particles with Ordered Inverse Bicontinuous Cubic and Hexagonal Mesophases. *ACS Nano* **2021**, *15*, 4688−4698.
(30) Wen, W.; Guan, S.; Yang, Z.; Chen, A. Inverse Bicontinuous Structure by Polymerization-Induced Self-Assembly Against Single-Chain Nanoparticles. *ACS Macro Lett.* **2021**, *10*, 603−608.
(31) Sadek, H.; Siddique, K. S.; Wang, C.-W.; Lee, C.-C.; Chang, S.-Y.; Ho, R.-M. Bioinspired Nanonetwork Hydroxyapatite from Block Copolymer Templated Synthesis for Mechanical Metamaterials. *ACS Nano* **2022**, *16*, 18298−18306.
(32) Yang, K. C.; Puneet, P.; Chiu, P. T.; Ho, R. M. Well-Ordered Nanonetwork Metamaterials from Block Copolymer Templated Syntheses. *Acc. Chem. Res.* **2022**, *55*, 2033−2042.
(33) Siddique, S. K.; Lin, T.-C.; Chang, C.-Y.; Chang, Y.-H.; Lee, C.-C.; Chang, S.-Y.; Tsai, P.-C.; Jeng, Y.-R.; Thomas, E. L.; Ho, R.-M. Nanonetwork Thermosets from Templated Polymerization for Enhanced Energy Dissipation. *Nano Lett.* **2021**, *21*, 3355−3363.
(34) Allen, S. D.; Bobbala, S.; Karabin, N. B.; Scott, E. A. On the advancement of polymeric bicontinuous nanospheres toward biomedical applications. *Nanoscale Horiz.* **2019**, *4*, 258−272.
(35) Wong, C. K.; Qiang, X.; Müller, A. H. E.; Gröschel, A. H. Self-Assembly of block copolymers into internally ordered microparticles. *Prog. Polym. Sci.* **2020**, *102*, No. 101211.
(36) Zhu, A.; Lv, X.; Shen, L.; Zhang, B.; An, Z. Polymerization-Induced Cooperative Assembly of Block Copolymer and Homopolymer via RAFT Dispersion Polymerization. *ACS Macro Lett.* **2017**, *6*, 304−309.
(37) Gao, C.; Wu, J.; Zhou, H.; Qu, Y.; Li, B.; Zhang, W. Self-Assembled Blends of AB/BAB Block Copolymers Prepared through Dispersion RAFT Polymerization. *Macromolecules* **2016**, *49*, 4490−4500.
(38) Yuan, B.; He, X.; Qu, Y.; Gao, C.; Eiser, E.; Zhang, W. In situ synthesis of a self-assembled AB/B blend of poly(ethylene glycol)-*b*-polystyrene/polystyrene by dispersion RAFT polymerization. *Polym. Chem.* **2017**, *8*, 2173−2181.
(39) Tan, J.; Huang, C.; Liu, D.; Li, X.; He, J.; Xu, Q.; Zhang, L. Polymerization-Induced Self-Assembly of Homopolymer and Diblock Copolymer: A Facile Approach for Preparing Polymer Nano-Objects with Higher-Order Morphologies. *ACS Macro Lett.* **2017**, *6*, 298−303.
(40) Huang, C.; Tan, J.; Xu, Q.; He, J.; Li, X.; Liu, D.; Zhang, L. Adding a solvophilic comonomer to the polymerization-induced self-assembly of block copolymer and homopolymer: a cooperative strategy for preparing large compound vesicles. *RSC Adv.* **2017**, *7*, 46069−46081.
(41) Galanos, E.; Grune, E.; Wahlen, C.; Mueller, A. H. E.; Appold, M.; Gallei, M.; Frey, H.; Floudas, G. Tapered Multiblock Copolymers Based on Isoprene and 4-Methylstyrene: Influence of the Tapered Interface on the Self-Assembly and Thermomechanical Properties. *Macromolecules* **2019**, *52*, 1577−1588.
(42) Grune, E.; Appold, M.; Mueller, A. H. E.; Gallei, M.; Frey, H. Anionic Copolymerization Enables the Scalable Synthesis of Alternating (AB)(n) Multiblock Copolymers with High Molecular Weight in n/2 Steps. *ACS Macro Lett.* **2018**, *7*, 807−810.
(43) Steube, M.; Johann, T.; Galanos, E.; Appold, M.; Ruettiger, C.; Mezger, M.; Gallei, M.; Mueller, A. H. E.; Floudas, G.; Frey, H. Isoprene/Styrene Tapered Multiblock Copolymers with up to Ten Blocks: Synthesis, Phase Behavior, Order, and Mechanical Properties. *Macromolecules* **2018**, *51*, 10246−10258.
(44) von Tiedemann, P.; Blankenburg, J.; Maciol, K.; Johann, T.; Mueller, A. H. E.; Frey, H. Gopolymerization of Isoprene with p-Alkylstyrene Monomers: Disparate Reactivity Ratios and the Shape of the Gradient. *Macromolecules* **2019**, *52*, 796−806.
(45) Yamauchi, K.; Hasegawa, H.; Hashimoto, T.; Tanaka, H.; Motokawa, R.; Koizumi, S. Direct observation of polymerization-reaction-induced molecular self-assembling process: In-situ and real-time SANS measurements during living anionic polymerization of polyisoprene-block-polystyrene. *Macromolecules* **2006**, *39*, 4531−4539.
(46) Tanaka, H.; Yamauchi, K.; Hasegawa, H.; Miyamoto, N.; Koizumi, S.; Hashimoto, T. In situ and real-time small-angle neutron scattering studies of living anionic polymerization process and polymerization-induced self-assembly of block copolymers. *Phys. B* **2006**, *385*, 742−744.
(47) Zhao, Y.; Miyamoto, N.; Koizumi, S.; Hashimoto, T. Combined SANS, SEC, NMR, and UV-vis Studies of Simultaneous

https://doi.org/10.1021/acs.macromol.3c00759
Macromolecules 2023, 56, 5743−5753

Living Anionic Copolymerization Process in a Concentrated Solution: Elucidation of Building-Up Processes of Molecules and Their Self-Assemblies. *Macromolecules* **2010**, *43*, 2948−2959.
(48) Boott, C. E.; Gwyther, J.; Harniman, R. L.; Hayward, D. W.; Manners, I. Scalable and uniform 1D nanoparticles by synchronous polymerization, crystallization and self-assembly. *Nat. Chem.* **2017**, *9*, 785−792.
(49) Oliver, A. M.; Gwyther, J.; Boott, C. E.; Davis, S.; Pearce, S.; Manners, I. Scalable Fiber-like Micelles and Block Co-micelles by Polymerization-Induced Crystallization-Driven Self-Assembly. *J. Am. Chem. Soc.* **2018**, *140*, 18104−18114.
(50) Wang, J.; Cao, M.; Zhou, P.; Wang, G. Exploration of a Living Anionic Polymerization Mechanism into Polymerization-Induced Self-Assembly and Site-Specific Stabilization of the Formed Nano-Objects. *Macromolecules* **2020**, *53*, 3157−3165.
(51) Zhou, C.; Wang, J.; Zhou, P.; Wang, G. A polymerization-induced self-assembly process for all-styrenic nano-objects using the living anionic polymerization mechanism. *Polym. Chem.* **2020**, *11*, 2635−2639.
(52) Chen, L.; Shen, H. W.; Eisenberg, A. Kinetics and mechanism of the rod-to-vesicle transition of block copolymer aggregates in dilute solution. *J. Phys. Chem. B* **1999**, *103*, 9488−9497.
(53) Glatter, O.; Kratky, O.; Kratky, H. *Small angle X-ray scattering*; Academic press, 1982.
(54) Roe, R.-J. *Methods of X-ray and neutron scattering in polymer science*; Oxford University Press on Demand, 2000.
(55) Warren, N. J.; Mykhaylyk, O. O.; Mahmood, D.; Ryan, A. J.; Armes, S. P. RAFT aqueous dispersion polymerization yields poly(ethylene glycol)-based diblock copolymer nano-objects with predictable single phase morphologies. *J. Am. Chem. Soc.* **2014**, *136*, 1023−1033.
(56) Schroder-Turk, G. E.; Varslot, T.; de Campo, L.; Kapfer, S. C.; Mickel, W. A bicontinuous mesophase geometry with hexagonal symmetry. *Langmuir* **2011**, *27*, 10475−10483.
(57) Lin, Z.; Liu, S.; Mao, W.; Tian, H.; Wang, N.; Zhang, N.; Tian, F.; Han, L.; Feng, X.; Mai, Y. Tunable Self-Assembly of Diblock Copolymers into Colloidal Particles with Triply Periodic Minimal Surfaces. *Angew. Chem., Int. Ed.* **2017**, *56*, 7135−7140.
(58) La, Y.; Park, C.; Shin, T. J.; Joo, S. H.; Kang, S.; Kim, K. T. Colloidal Inverse Bicontinuous Cubic Membranes of Block Copolymers with Tunable Surface Functional Groups. *Nat. Chem.* **2014**, *6*, 534−541.
(59) Demurtas, D.; Guichard, P.; Martiel, I.; Mezzenga, R.; Hébert, C.; Sagalowicz, L. Direct Visualization of Dispersed Lipid Bicontinuous Cubic Phases by Cryo-Electron Tomog raphy. *Nat. Commun.* **2015**, *6*, 8915.
(60) La, Y.; Song, J.; Jeong, M. G.; Cho, A.; Jin, S.-M.; Lee, E.; Kim, K. T. Templated Synthesis of Cubic Crystalline Single Networks Having Large Open-Space Lattices by Polymer Cubosomes. *Nat. Commun.* **2018**, *9*, 5327.
(61) Zhang, L. F.; Yu, K.; Eisenberg, A. Ion-induced morphological changes in "crew-cut" aggregates of amphiphilic block copolymers. *Science* **1996**, *272*, 1777−1779.
(62) Zhang, L. F.; Eisenberg, A. Morphogenic effect of added ions on crew-cut aggregates of polystyrene-b-poly(acrylic acid) block copolymers in solutions. *Macromolecules* **1996**, *29*, 8805−8815.
(63) Khor, S. Y.; Quinn, J. F.; Whittaker, M. R.; Truong, N. P.; Davis, T. P. Controlling Nanomaterial Size and Shape for Biomedical Applications via Polymerization-Induced Self-Assembly. *Macromol. Rapid Commun.* **2019**, *40*, No. e1800438.
(64) Saviano, M.; Aquino, R. P.; Del Gaudio, P.; Sansone, F.; Russo, P. Poly(vinyl alcohol) 3D printed tablets: The effect of polymer particle size on drug loading and process efficiency. *Int. J. Pharm.* **2019**, *561*, 1−8.
(65) Zeng, M.; Li, X.; Zhang, Y.; Chen, X.; Sui, X.; Yuan, J. Tailoring the droplet size of Pickering emulsions by PISA synthesized polymeric nanoparticles. *Polymer* **2020**, *206*, No. 122853.
(66) Nanda, T.; Singh, K.; Shelly, D.; Mehta, R. Advancements in multi-scale filler reinforced epoxy nanocomposites for improved impact strength: A review. *Crit. Rev. Solid State Mater. Sci.* **2020**, *46*, 281−329.

https://doi.org/10.1021/acs.macromol.3c00759
Macromolecules 2023, 56, 5743−5753